

Supplement

Hydrothermal trace metal release and microbial metabolism in the Northeast Lau Basin of the south Pacific Ocean

Natalie R. Cohen^{1,2}, Abigail E. Noble¹, Dawn M. Moran¹, Matthew R. McIlvin¹, Tyler J. Goepfert^{1,3}, Nicholas J. Hawco⁴, Christopher R. German¹, Tristan J. Horner¹, Carl H. Lamborg⁵, John P. McCrow⁶, Andrew E. Allen⁶, and Mak A. Saito¹

¹ Woods Hole Oceanographic Institution, Woods Hole MA 02543 USA

² University of Georgia Skidaway Institute of Oceanography, Savannah GA 31411 USA

³ Arizona State University, Tempe AZ 85281 USA

⁴ University of Hawai'i at Mānoa, Honolulu HI 96822 USA

⁵ University of California, Santa Cruz, Santa Cruz, CA 95064 USA

⁶ J. Craig Venter Institute, La Jolla CA 92037 USA

Correspondence to: Natalie R. Cohen (cohen@uga.edu) or Mak A. Saito (msaito@whoi.edu)

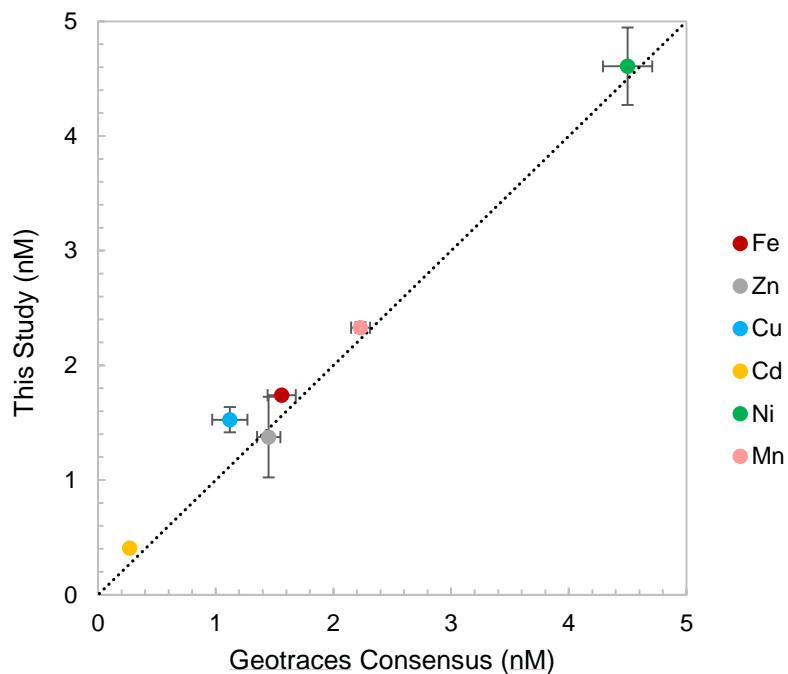


Fig. S1. Comparison of Geotraces coastal surface seawater (GSC) standard concentrations between this study (n=3) and the Geotraces community consensus, as shown in Table 1. The dotted line shows a 1:1 relationship. Vertical and horizontal error bars represent the standard deviation.

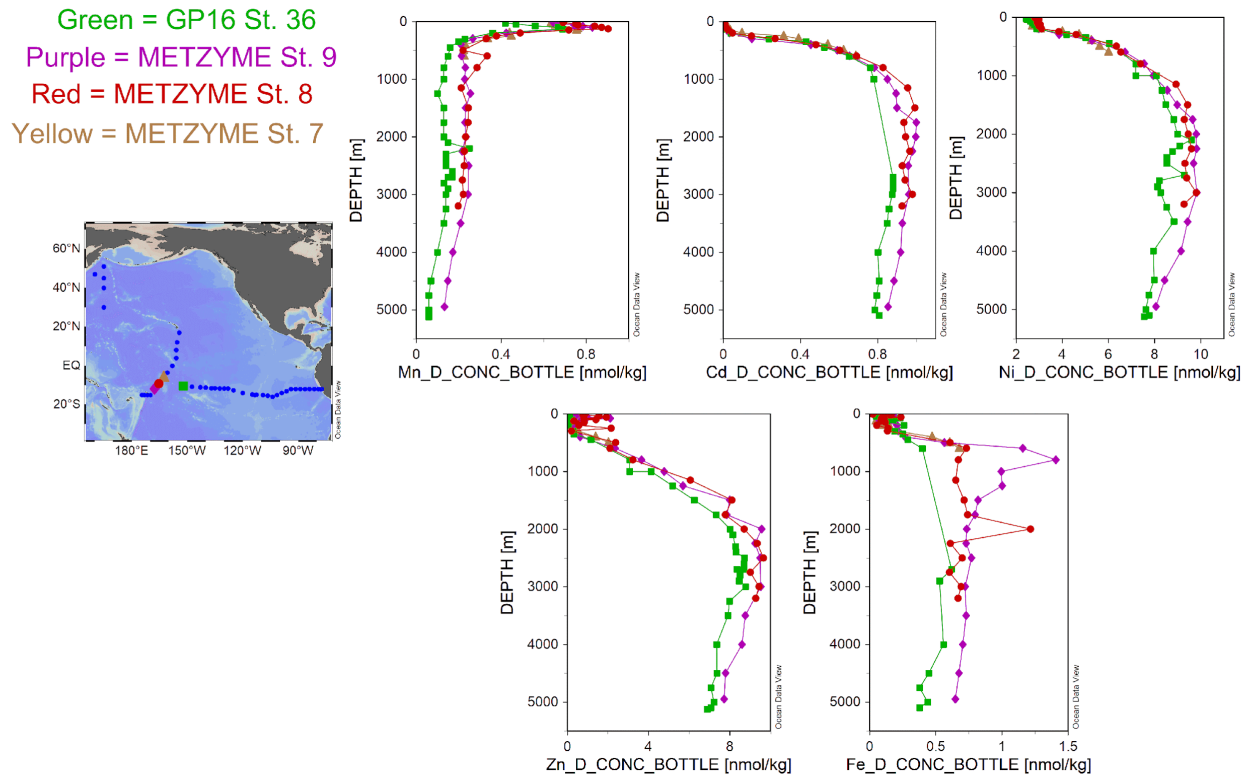


Fig. S2. Dissolved metal profiles obtained in this study compared to the closest station of the GP16 cruise, which sampled approximately 1,000 km east of the Metzyme transect in the South Pacific. The profiles show overall similar distributions, with slight offsets at depth for Zn, Cd and Ni. Fe profiles are elevated at our St. 9 which we hypothesize is due to hydrothermal influence. The Fe and Cd concentrations are from John et al. (2017) and (2018) (<https://www.bco-dmo.org/dataset/643809>), and Zn, Ni, and Mn from the Bruland data set (<https://www.bco-dmo.org/dataset-deployment/643427>).

John, S. G., J. Helgoe, and E. Townsend. 2017. Biogeochemical cycling of Zn and Cd and their stable isotopes in the Eastern Tropical South Pacific. *Mar. Chem.* 0–1. doi:10.1016/j.marchem.2017.06.001

John, S. G., J. Helgoe, E. Townsend, and others. 2018. Biogeochemical cycling of Fe and Fe stable isotopes in the Eastern Tropical South Pacific. *Mar. Chem.* **201**: 66–76. doi:10.1016/j.marchem.2017.06.003

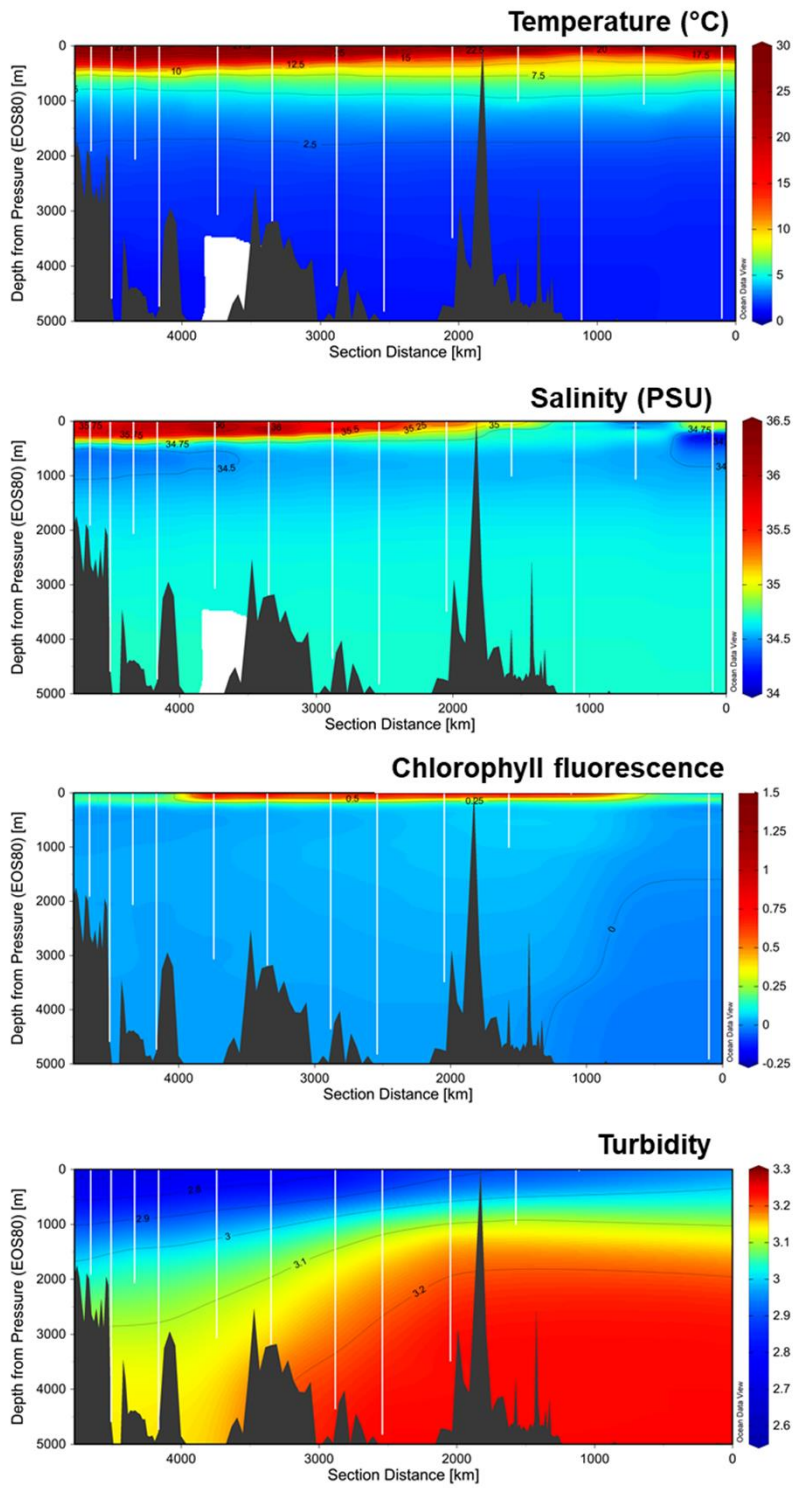


Fig. S3. Temperature, salinity, fluorescence, and turbidity sections from the trace metal rosette CTD, plotted using weighted-gridding interpolation in Ocean Data View.

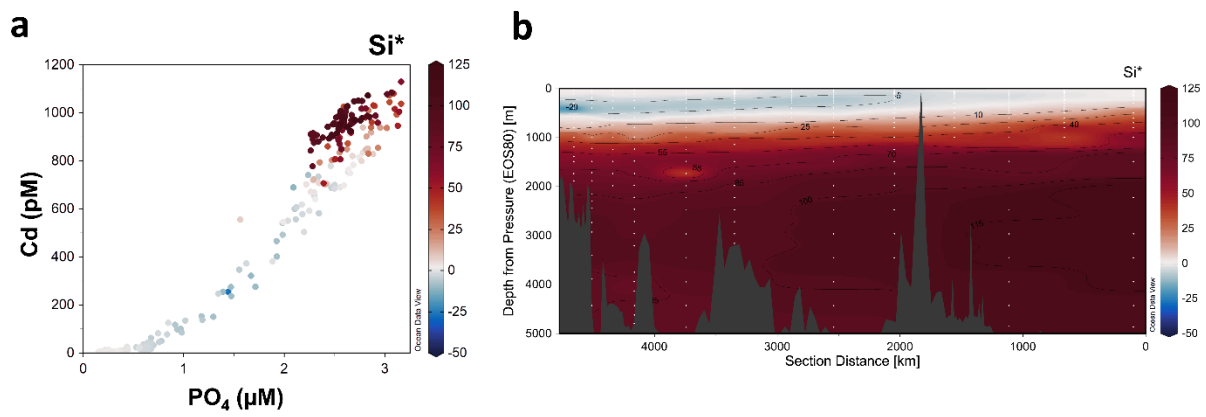


Fig. S4. (a) Cd and PO₄ relationship in the Metzyme dataset, colored by Si* (dSi – dNO₃). (b) Si* highlighting Antarctic-sourced surface seawater across the Metzyme section.

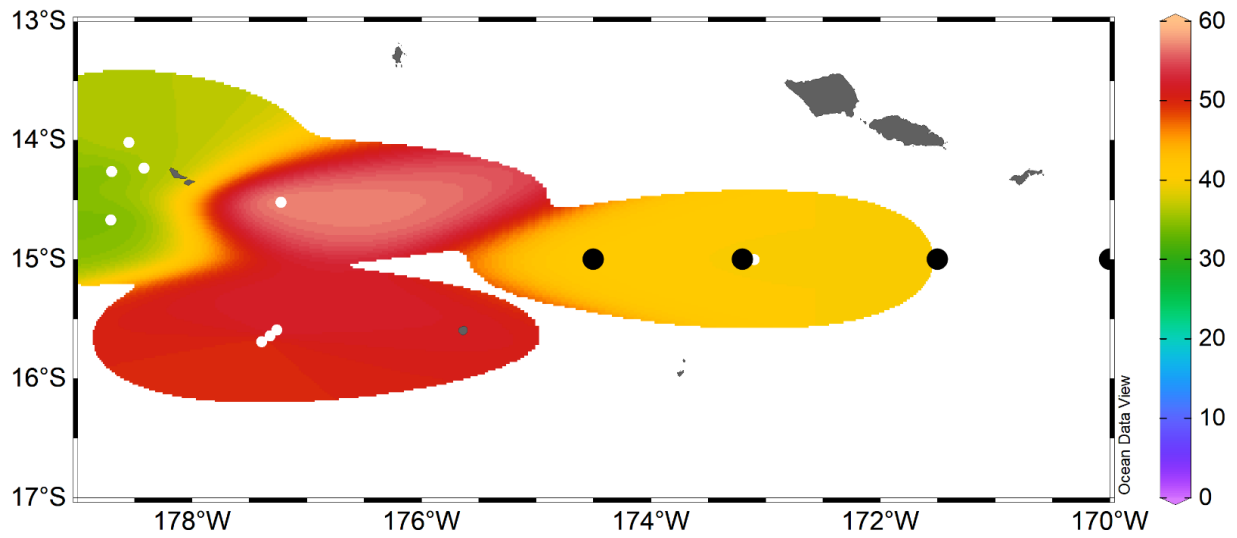


Fig. S5. $\delta^3\text{He}$ in the southwest Pacific at 1,900m collected from the Global Oceanic Database of Tritium and Helium (Jenkins et al. 2019), plotted in Ocean Data View. $\delta^3\text{He}$ data points are shown in white, Metzyme stations are shown in black.

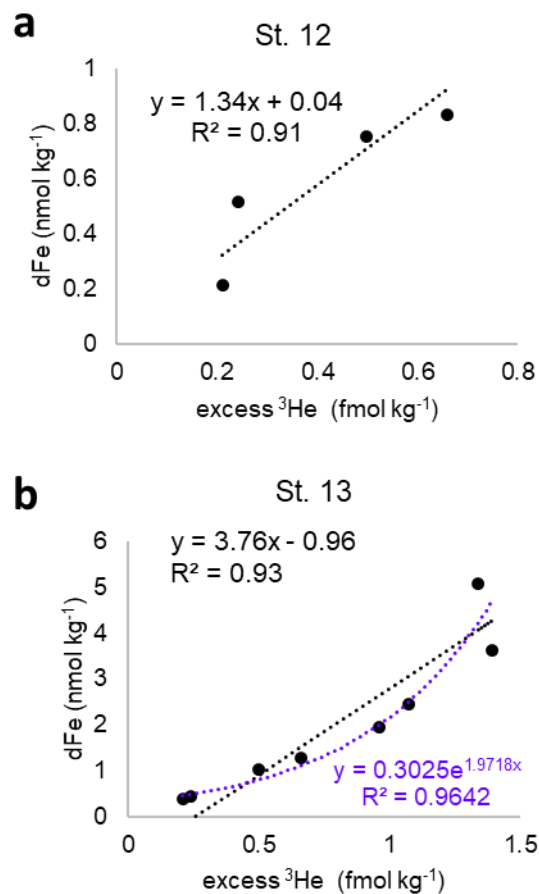


Fig. S6. (a) Estimated relationship between dissolved iron and excess helium in the NE Lau Basin using $\delta^3\text{He}$ reported in Lupton et al. (2004) at the same coordinates as Metzyme St. 12, and iron concentrations from St. 12. For comparison, the $d\text{Fe}:\text{}^3\text{He}$ ratio obtained using Fe concentrations from St. 13 is shown in Fig 5C. A Type II linear regression is plotted (Glover et al., 2012). Total He and Ne concentrations were not available and were estimated for this region (Jenkins et al., 2019a). Upper water column ^3He concentrations were extrapolated using historical data from Lupton et al. (2004). St. 12 has two Fe maxima, neither of which align with the 1,726 m ^3He maximum, and therefore only the top of the profile is used in the regression. **(b)** The relationship between dFe measured at St. 13 and ^3He from Lupton et al. (2004) shown in Fig. 5C alongside an exponential curve fit (in purple). Although the exponential fit is supported by a high R^2 value, it is largely driven by one data point.

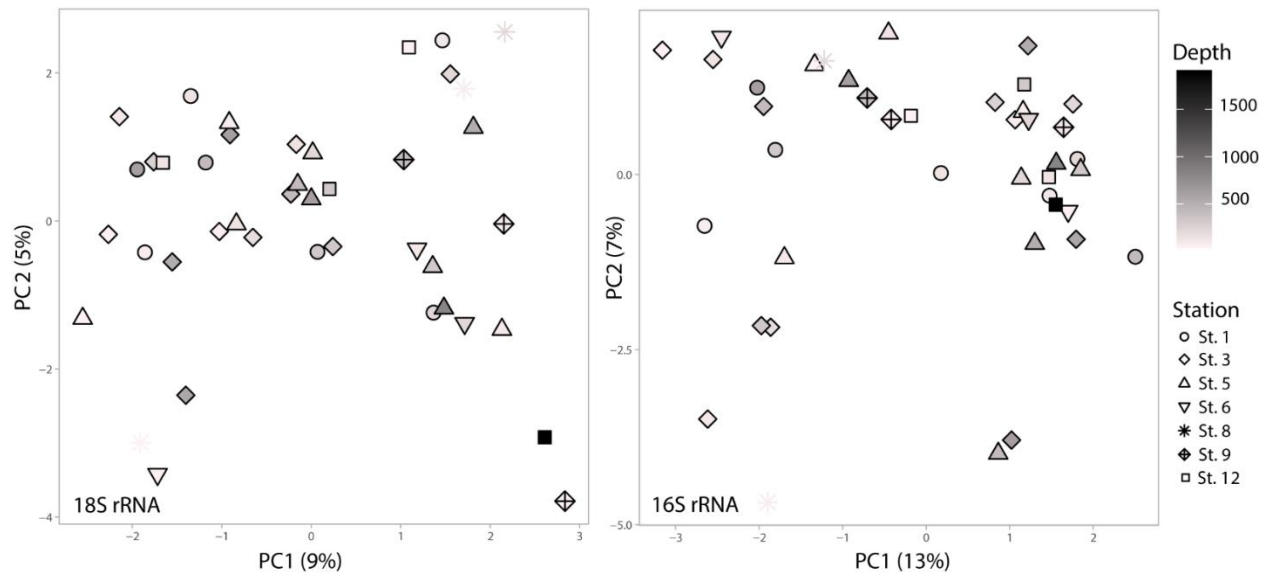


Fig. S7. Principal coordinate analysis (PCoA) of 18S rRNA (left) and 16S rRNA (right) OTUs using Bray-Curtis dissimilarity within the R package *vegan*. OTUs were center-log-ratio transformed. The color scale represents surface to deep, with the hydrothermal distal plume sample in black. Each station is represented by a unique shape. Axes show the percent variation explained by each eigenvalue. These 16S rRNA and 18S rRNA data sets were published in Cohen et al. 2021.

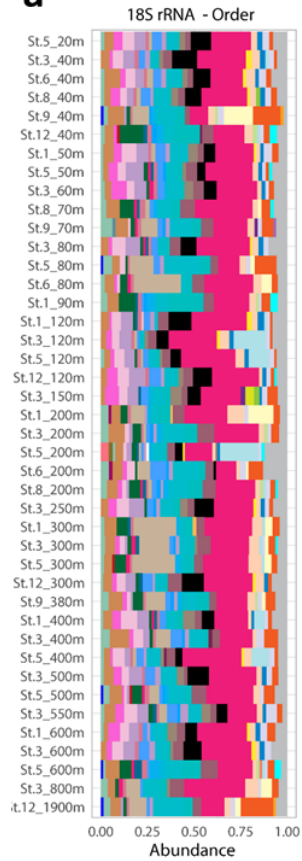
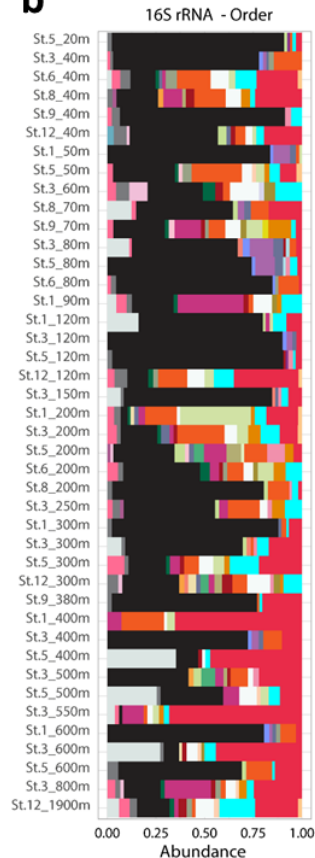
a**b**

Fig. S8. Order-level community composition based on 18S rRNA OTU (top) and 186 rRNA OTU (bottom) relative abundance, depicted as stacked bar plots. Low abundance taxa contributing to less than 1% of the community were removed. Higher class or supergroup identification is indicated in parentheses. If no order-level assignment was available, the lowest classification was provided. These 16S rRNA and 18S rRNA data sets were published in Cohen et al. 2021.

Table S1. Metzyme sampling stations, depths, flow volumes, and protein concentrations.

Table S2. Metaproteomic spectral counts associated with proteins detected in deep waters (≥ 200 m). Only peptide spectral counts matching open reading frames (ORFs) with a classified taxonomic annotation and lineage probability index greater than 0.7 are shown. Exclusive spectral counts were normalized following the NSAF (normalized spectral abundance factor) approach. Relative abundance of proteins in the plume (St. 12, 1,900m) was compared to background deep sites (n=20) using a permutation test followed by Benjamini-Hochberg multiple test correction. Blue rows indicate differentially abundant proteins in hydrothermally-influenced seawater (FDR < 0.1).